Macroporous Catalysts

DOI: 10.1002/anie.201107981

Facile Oxygen Reduction on a Three-Dimensionally Ordered Macroporous Graphitic C_3N_4/Carbon Composite Electrocatalyst**

*Ji Liang, Yao Zheng, Jun Chen, Jian Liu, Denisa Hulicova-Jurcakova, Mietek Jaroniec, and Shi Zhang Qiao**

One of the greatest stumbling blocks hindering broad applications of fuel cells is the high cost and vulnerability of the platinum catalyst as well as the sluggish oxygen reduction reaction (ORR) on the cathode.[1] Although Pt alloys or non-noble metals have been developed as substitute catalysts for the ORR,[2,3] they still suffer from multiple disadvantages, such as low stability under fuel cell conditions, vulnerability to fuel crossover, and harmfulness to the environment.[4] Thus, the ongoing search for metal-free catalysts for the ORR has attracted much attention. In this regard, nitrogen-containing carbon materials are of particular interest owing to their catalytic activity towards the ORR brought about by nitrogen incorporation, which has been confirmed by both experimental studies[5–7] and quantum-mechanical calculations.[8] Among these materials, graphitic carbon nitride (g-C_3N_4) is especially promising because of its high nitrogen content, low cost, and easily tailorable structure,[9] which makes it potentially suitable for oxygen reduction as well as other applications, such as photocatalysis[10] or hydrogen storage, under mild conditions.[11]

However, the ORR electrocatalytic activity of g-C_3N_4 alone is still inferior to Pt catalysts.[12,13] This is because of the extremely low electrical conductivity (ca. 10^{-9} S m^{-1} [10,14]) of g-C_3N_4 as indicated by our recent theoretical calculations.[15] With the aim to better utilize this nitrogen-rich but poorly conducting material, a variety of carbon materials have been recently introduced into g-C_3N_4 by different routes, including mechanical mixing of g-C_3N_4 with carbon black[16] or in situ immobilization of g-C_3N_4 onto carbon black,[17] graphene,[13,18] or mesoporous carbon.[15] Compared to pristine g-C_3N_4, the aforementioned composites show better catalytic performance for ORR (that is, higher cathodic reaction current or lower ORR starting potential in a half-cell test). However, the effect of the structure of these composites on the catalytic properties is still unknown.

The porosity of catalyst in a fuel cell is critical for mass transport and access of the proton exchange ionomers.[19,20] However, the pores of previously investigated g-C_3N_4/carbon materials (g-C_3N_4/C) arise from pyrolysis of carbon precursors,[16,17] random stacking of graphene layers,[13,18] or mesoporous carbon with small pores.[15] The pore sizes of these composites are hard to control and often too narrow for efficient transport and access.[19,20] Furthermore, the potential prospects of g-C_3N_4/C as a substitute for Pt cannot be forecast on the basis of the current research because the ORR catalytic activity of the existing g-C_3N_4/C is hardly comparable to Pt[16–18] and/or they are not stable enough in the fuel cell environments.[13]

From this point of view, a more uniform structure with suitable pore size of the carbon substrate could be preferable for hybrid g-C_3N_4/C fuel cell catalysts. More specifically, a well-defined and continuous porous structure would facilitate reactant transport inside the pores, assure better contact between catalyst and ionomer, and better stability, as well as create an opportunity for an accurate evaluation of the structural effect of the added carbon on the ORR catalytic properties of g-C_3N_4/C. On this basis, a hard template method using silica microspheres as templates can be especially feasible and advantageous for preparing the carbon supports for g-C_3N_4 in several aspects. Preparation of g-C_3N_4/C with tunable pore size from meso to macropores could be easily achieved using this method.[21–27] Besides, the carbon materials thus synthesized feature uniform cage-like interconnected pores, which not only facilitate the mass transport but also avoid possible confusion in assessing the effect of pore sizes due to structural differences. Furthermore, this three-dimensionally interconnected structure would be stronger than the microscopically separated carbon materials, and the silica spheres are either commercially available or easy to fabricate, making the resulting g-C_3N_4/C potentially favorable for commercialization at low cost.

Herein we present the design and preparation of macroporous g-C_3N_4/C with three-dimensionally ordered interconnected structures using silica microspheres as hard templates. The main objective is to develop a high performance metal-free fuel cell catalyst, to evaluate the structural effect of the

[*] J. Liang, Y. Zheng, Dr. J. Liu, Dr. D. Hulicova-Jurcakova, Prof. S. Z. Qiao
ARC Centre of Excellence for Functional Nanomaterials
Australian Institute for Bioengineering and Nanotechnology
The University of Queensland, QLD 4072 (Australia)
E-mail: s.qiao@uq.edu.au
Prof. S. Z. Qiao
School of Chemical Engineering
The University of Adelaide, SA 5005 (Australia)
Dr. J. Chen
Intelligent Polymer Research Institute
ARC Centre of Excellence for Electromaterials Science
Australian Institute of Innovative Materials
University of Wollongong, NSW 2522 (Australia)
Prof. M. Jaroniec
Department of Chemistry and Biochemistry
Kent State University, Kent, OH 44242 (USA)

[**] This work is financially supported by the Australian Research Council (ARC) through the Discovery Project program (DP1095861, DP0987969).

Supporting information for this article is available on the WWW under http://dx.doi.org/10.1002/anie.201107981.

resulting g-C_3N_4/C on the electrocatalytic activity as well as to reveal its potential suitability as a substitute for Pt/C used in fuel cells. The catalytic activity of g-C_3N_4/C for ORR has been measured in comparison with mesoporous g-C_3N_4/C and commercial Pt/C. The g-C_3N_4/C catalysts with ordered pores of about 150 nm showed highest ORR performance, which was comparable with Pt/C in both the reaction current and the initial potential. Moreover, unlike the vulnerable commercial Pt/C, our material had extremely high tolerance against fuel crossover. Furthermore, this macroporous g-C_3N_4/C catalyst also possessed an excellent durability compared to both commercial Pt/C and previously reported g-C_3N_4/C in alkaline media.[13,18] To our knowledge, all of these properties have not been achieved in other metal-free catalysts, which make the current macroporous g-C_3N_4/C catalyst promising for the next generation of alkaline fuel cells based on organic fuels.

Macroporous g-C_3N_4/C was prepared as shown in Figure 1 a. Silica spheres with different sizes were synthesized by

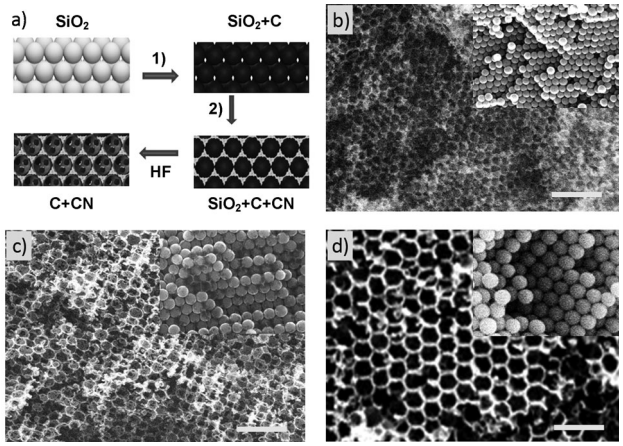

Figure 1. a) The synthesis of macroporous g-C_3N_4/C as a reversal of the SiO_2 sphere structure. Conditions: 1) Sucrose, 900 °C, N_2; 2) cyanamide, 550 °C, N_2. b)–d) Scanning electron microscopy (SEM) images of 150-C/CN, 230-C/CN, and 400-C/CN (and the corresponding silica spheres of each size (insets). Scale bars: 1 μm.

Stober's method[28] and packed up by gravitational sedimentation or solvent vaporization, forming an opal monolith. The monolith was then dried and calcined at 550 °C to obtain interconnected silica spheres. In the next step, a thin carbon shell was coated on the silica spheres (C@SiO_2) through sucrose infiltration followed by carbonization at 900 °C in nitrogen (Supporting Information, Figure S1). Afterward, melted cyanamide, as g-C_3N_4 precursor, was impregnated into the intersphere spaces of C@SiO_2, followed by heating at 550 °C in nitrogen to form g-C_3N_4/C@SiO_2. Finally, the silica template was removed with hydrofluoric acid after g-C_3N_4 synthesis, rather than in earlier stages, which successfully prevented the possible structural deterioration and pore blockage. Noticeably, as-synthesized g-C_3N_4/C (denoted as X-C/CN, where X is the pore size) has well-defined interconnected ordered macropores with the same size as the silica spheres (Figure 1).

The formation of g-C_3N_4 in the composite is confirmed by X-ray diffraction (XRD) on the basis of the peaks at 2θ located at 30° and 52° and corresponding to the (002) and the (101) face (Figure 2 a).[9] The existence of g-C_3N_4 on carbon is

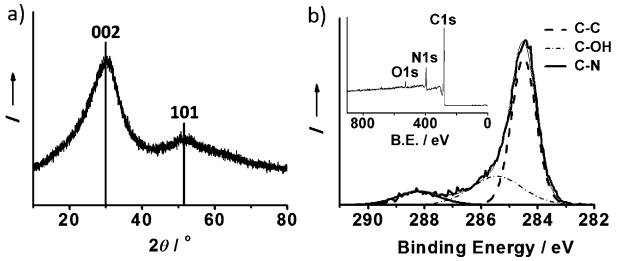

Figure 2. a) Typical XRD pattern obtained by Co Kα X-rays; b) typical high-resolution C 1s XPS spectrum. Inset: corresponding survey scan of g-C_3N_4/C.

also evidenced by FTIR spectra on the basis of characteristic g-C_3N_4 absorbance peaks (Supporting Information, Figure S2). X-ray photoelectron spectroscopy (XPS) is another method to probe the integration of g-C_3N_4 with carbon. The survey scan spectrum of g-C_3N_4/C shows the presence of carbon, nitrogen, and oxygen (inset in Figure 2 b). High resolution C1 s spectra reveal the carbon status in the material (Figure 2 b). The emergence of the peak at 288.3 eV corresponding to C–N coordination and the enhancement of the peak at 284.5 eV corresponding to C–C coordination, compared to pristine carbon and g-C_3N_4 (Supporting Information, Figure S3), confirm the successful incorporation of g-C_3N_4 onto carbon.[13,16] Another peak at 285.7 eV corresponds to C–OH, which is from the sucrose precursor and is commonly observed on carbon materials.[29] High-resolution scans of N 1s in g-C_3N_4/C and g-C_3N_4 show similar nitrogen species, indicating comparable nitrogen status in both materials (Supporting Information, Figure S3). The porosity of these materials was investigated by nitrogen sorption measurements. As a result, all of the macroporous samples possess similar Brunauer–Emmett–Teller (BET) specific surface areas in the range between 50 and 100 $m^2 g^{-1}$; the surface area tends to decrease with increasing pore size (Supporting Information, Figure S5). No significant presence of mesopores or micropores was observed.

To further evaluate the pore size effect on the ORR catalytic activity of g-C_3N_4/C, mesoporous g-C_3N_4/C was also prepared for the purpose of comparison. The fabrication was firstly carried out by synthesizing mesoporous carbon using 12 nm colloidal silica spheres as a hard template as previously reported.[24] Cyanamide was then cast into the mesoporous carbon followed by heating at 550 °C, forming g-C_3N_4 inside mesoporous carbon (denoted as 12-C/CN). Both the 12-C/CN and the mesoporous carbon have the similar isotherm hysteresis loop confirming the presence of mesopores, but slight pore shrinkage is observed in 12-C/CN as compared to the parent carbon material (Supporting Information, Figure S6). These results indicate that both mesoporous materials possess similar cage like pores and g-C_3N_4 impregnation into mesoporous carbon does not significantly change its pore

structure. Transmission electron microscopy (TEM) observation also confirms the similar structures of mesoporous g-C_3N_4/C and carbon (Supporting Information, Figure S6). The uniform mesoporous structure of 12-C/CN is extremely suitable for comparison with its macroporous counterparts under study.

The ORR electrocatalytic activity of g-C_3N_4/C was firstly tested through conventional three-electrode cyclic voltammetry (CV) in O_2 or N_2 saturated 0.1 M KOH aqueous solutions (Figure 3a). A voltammogram without any significant peak was obtained in the absence of oxygen. The quasi-rectangular shape is due to a capacitor effect.[6,7] On the contrary, when oxygen was introduced, a characteristic ORR peak starting at −0.177 V was observed, showing the electrochemical reduction of oxygen initiated on g-C_3N_4/C. Compared to previous reports on nitrogen-doped carbon materials, the starting potential has increased positively,[6,30,31] indicating an easier ORR process on g-C_3N_4/C. At the same time, pure g-C_3N_4 with similar structure was also tested under the same conditions, showing the negligible ORR catalytic activity. The results indicate that the performance enhancement of g-C_3N_4/C was brought about by the introduction of carbon (Supporting Information, Figure S7).

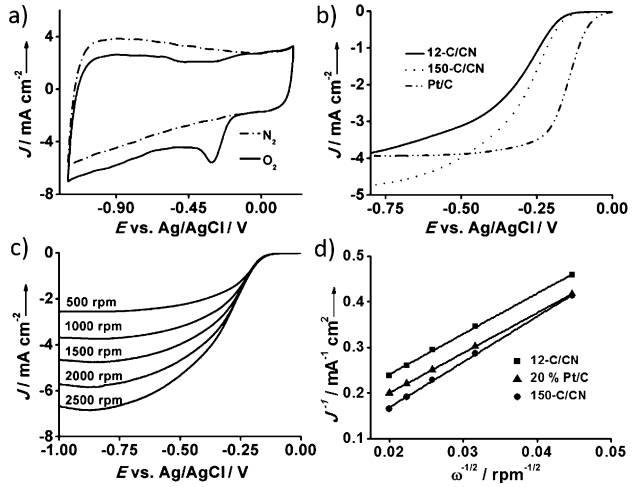

Figure 3. Catalytic activity towards electrochemical reduction of oxygen in 0.1 M KOH aqueous solution at room temperature. a) Cyclic voltammetry performed for 150-C/CN in O_2 and N_2; b) onset potential of mesoporous (12-C/CN), macroporous (150-C/CN) g-C_3N_4/C, and Pt/C obtained with a rotating disk electrode (RDE) at 1500 rpm and 5 mVs^{-1}; c) linear sweep voltammograms (LSVs) obtained for macroporous g-C_3N_4/C (150-C/CN) at various speeds; d) Koutecky–Levich plot for g-C_3N_4/C and Pt/C obtained from LSVs in (c) and the Supporting Information, Figure S7 at −0.6 V.

To further investigate the ORR catalytic activity of g-C_3N_4/C and the effect of pore size, these materials and commercial Pt/C (Vulcan, 20 wt%) were tested using a rotating disk electrode (RDE) in O_2-saturated 0.1 M KOH solution. The g-C_3N_4 amounts in each sample on the electrode in the RDE tests were the same by carefully controlling the catalyst ink concentration according to the elemental and thermogravimetric analysis results (Supporting Information, Figure S8 and Table S2). The ORR onset potentials of each sample were acquired from RDE linear sweep at 1500 rpm (Figure 3b). Remarkably, the macroporous g-C_3N_4/C showed obviously better performance than the mesoporous material in both onset potential (ca. −0.14 V) and reaction current density, which is comparable to Pt/C and indicates better performance brought about by larger pores.

Linear sweep voltammograms (LSV) were also recorded from 500 to 2500 rpm. LSVs for all g-C_3N_4/Cs show typical increasing current with higher rotations speeds (Figure 3c; Supporting Information, Figure S9). This result can be explained by shortened diffusion distance at high speeds, which is in accordance with other studies.[6,7] Noticeably, 12-C/CN showed a simultaneously increasing current density along with overpotential at all rotation speeds (Supporting Information, Figure S8), indicating a surface dominant reaction without a diffusion limited current, which is possibly due to the difficulties in reactant transfer within narrow 12 nm mesopores. The slight decrease in the current density at high rotation (2500 rpm) and high overpotential (> 0.9 V) might be caused by the fast O_2 consumption in the test cell.

The Koutecky–Levich plots (J^{-1} vs $\omega^{-1/2}$) of each catalyst are obtained from LSVs according to the current at −0.6 V, and all plots show good linearity at various rotation speeds (Figure 3d; Supporting Information, Figure S8). The macroporous samples exhibit higher current density than the mesoporous sample, and the 150-C/CN possesses the highest current density among all of the samples, which is even higher than that obtained for Pt/C at all rotation speeds (Figure 3b,d; Supporting Information, Figure S9), revealing the outstanding catalytic activity of this macroporous g-C_3N_4/C. The electron transfer numbers of ORR on different g-C_3N_4/C samples can be obtained from the slope of Koutecky–Levich plots (see details in the Supporting Information; these numbers are listed in Table S1).[32] All of the the g-C_3N_4/C samples possess a similar value of about 3, indicating a reasonably similar oxygen reduction process with combined two-electron and four-electron reaction pathways.[32]

To obtain insight into the ORR catalytic kinetic differences on g-C_3N_4/C with different pore sizes, the Tafel slopes, representing the overall resistance in the ORR process, were obtained according to the linear plots of LSVs at 1500 rpm for all g-C_3N_4/Cs (Figure 4a; Supporting Information, Figure S10). All of the plots show typical two-stage linear regions at low overpotential (> −0.2 V) and high overpotential (< −0.25 V), and the slope values are listed in Figure 4b.

In the low-overpotential region, where the overall ORR speed is determined by the surface reaction rate on the catalyst,[33] all of the Tafel slopes were between 51.1 and 72.6 mVdec^{-1}. The comparable values of the Tafel slopes for g-C_3N_4/C are also in agreement with their similar electron transfer numbers. This is in accordance with the fact that all g-C_3N_4/C can electrochemically reduce oxygen by a similar oxygen reduction process mechanism combining two- and four-electron reaction pathways. In the high overpotential region, where the overall ORR rate is dependent on the oxygen diffusion, the Tafel slope values for macroporous g-C_3N_4/Cs are between 150 and 190 mVdec^{-1}, which are much smaller than that of 12-C/CN (308 mVdec^{-1}), confirming

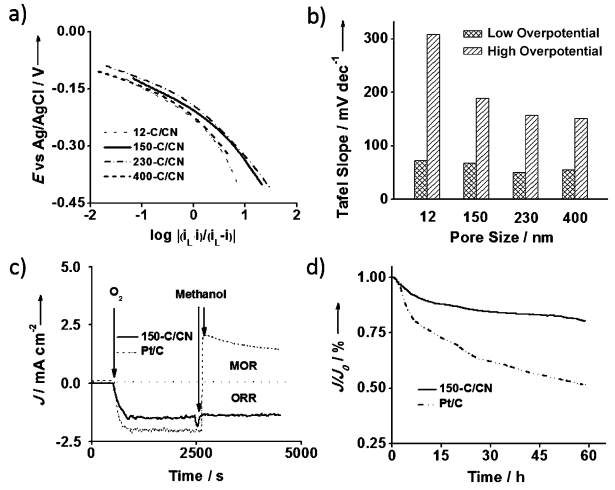

Figure 4. a) Tafel plots obtained from the RDE measurements on g-C_3N_4/C at 1500 rpm and b) the corresponding slope values of low and high overpotential regions; c) current–time chronoamperometric response of 150-C/CN and Pt/C in 0.1 M KOH solution. The arrow indicates the introduction of O_2 and 10 vol% methanol; d) current–time chronoamperometric response of 150-C/CN and Pt/C in O_2-saturated 0.1 M KOH solution.

significantly smoother reactant diffusion in the macropores than that in mesopores. As all of the samples show similar ORR mechanism at low overpotential, it is reasonable to assume that the better ORR activity of macroporous g-C_3N_4/C, compared to the mesoporous sample, is caused by the facile mass transfer in macropores. The superior performance of 150-C/CN could be the combination of both the positive effect of macropores on diffusion and the sufficient amount of active sites linked to the highest BET surface area among all macroporous samples.

For a new ORR electrocatalyst for fuel cells, a high catalytic selectivity for cathode reactions against fuel oxidation is important, especially when using small-molecule organic fuels, such as methanol, which could cross over through the polymer electrolyte membrane from anode to cathode, seriously compromising the whole cell performance.[13,31] The methanol crossover effect was evaluated on both macroporous g-C_3N_4/C and commercial Pt/C (Figure 4c). A negative current appeared when oxygen was introduced to N_2-saturated 0.1M KOH aqueous solution at about 500 s, indicating ORR occurred on both g-C_3N_4/C and Pt/C. After adding 10 vol% methanol to the electrolyte, g-C_3N_4/C retained stable current response whereas the current in the Pt/C system instantaneously jumped to positive values owing to the methanol oxidation reaction (MOR) on Pt/C. These results clearly show the excellent catalytic selectivity of g-C_3N_4/C and its better suitability as a cathode catalyst for direct methanol fuel cells than the vulnerable Pt/C.

The durability of g-C_3N_4/C and Pt/C was also assessed through chronoamperometric measurements at −0.3 V; at this potential the current was the largest, indicating the highest reaction rate (Figure 4d). The 100 h test only caused slight activity loss (reaction current decrease) on g-C_3N_4/C, whereas Pt/C lost nearly 50% of its initial activity in just 60 h, confirming a much better stability of active reaction sites on the g-C_3N_4/C materials than that on commercial Pt/C in alkaline environment, which is favored for the next generation alkaline fuel cells.

Taking into account the similar composition of the g-C_3N_4/C catalysts in this study and previous reports,[13] the observed enhancement in the ORR durability on the macroporous g-C_3N_4/C can be attributed to their uniquely porous structure. The composite catalyst synthesized in our study have a three-dimensionally interconnected porous structure, which effectively prevent the structural collapse or catalyst detachment that happens on microscopically separated carbon supported Pt or g-C_3N_4 catalysts, and thus help to keep our g-C_3N_4/C far more stable than other g-C_3N_4/C materials or commercial Pt/C.[13]

In summary, we have successfully designed and constructed a three-dimensionally ordered macroporous g-C_3N_4/C catalyst with outstanding ORR performance for fuel cells. This novel catalyst possesses prominent ORR catalytic activity, which is comparable with commercial Pt/C in both reaction current density and onset potential. As a metal-free catalyst, the macroporous g-C_3N_4/C showed much better fuel crossover resistance and long-term durability than the commercial Pt/C in alkaline medium. Furthermore, this material was synthesized through a simple procedure using inexpensive cyanamide as a precursor and easily fabricated silica microspheres as a template, which gives a great promise for large scale production. The pore size of g-C_3N_4/C can be easily tailored by using different size silica spheres as templates. All these features make macroporous g-C_3N_4/C a potentially promising and suitable substitute for the expensive noble metal catalysts in the next generation alkaline and direct methanol fuel cells.

Received: November 13, 2011
Published online: March 2, 2012

Keywords: carbon nitride · graphitic materials · heterogeneous catalysis · macroporous catalysts · oxygen reduction reaction

[1] B. C. H. Steele, A. Heinzel, *Nature* **2001**, *414*, 345.
[2] R. Bashyam, P. Zelenay, *Nature* **2006**, *443*, 63.
[3] H. Gasteiger, N. Markovi, *Science* **2009**, *324*, 48.
[4] D. S. Yu, E. Nagelli, F. Du, L. M. Dai, *J. Phys. Chem. Lett.* **2010**, *1*, 2165.
[5] K. Gong, F. Du, Z. Xia, M. Durstock, L. Dai, *Science* **2009**, *323*, 760.
[6] W. Yang, T.-P. Fellinger, M. Antonietti, *J. Am. Chem. Soc.* **2011**, *133*, 206.
[7] R. Liu, D. Wu, X. Feng, K. Müllen, *Angew. Chem.* **2010**, *122*, 2619; *Angew. Chem. Int. Ed.* **2010**, *49*, 2565.
[8] S. Maldonado, K. J. Stevenson, *J. Phys. Chem. B* **2005**, *109*, 4707.
[9] S. Hwang, S. Lee, J.-S. Yu, *Appl. Surf. Sci.* **2007**, *253*, 5656.
[10] X. Wang, K. Maeda, A. Thomas, K. Takanabe, G. Xin, J. M. Carlsson, K. Domen, M. Antonietti, *Nat. Mater.* **2009**, *8*, 76.
[11] S. S. Park, S. W. Chu, C. Xue, D. Zhao, C. S. Ha, *J. Mater. Chem.* **2011**, *21*, 10801.
[12] K. Kwon, Y. J. Sa, J. Y. Cheon, S. H. Joo, *Langmuir* **2012**, *28*, 991.

[13] S. Yang, X. Feng, X. Wang, K. Müllen, *Angew. Chem.* **2011**, *123*, 5451; *Angew. Chem. Int. Ed.* **2011**, *50*, 5339.
[14] Y. Zhang, T. Mori, J. Ye, M. Antonietti, *J. Am. Chem. Soc.* **2010**, *132*, 6294.
[15] Y. Zheng, Y. Jiao, J. Chen, J. Liu, J. Liang, A. Du, W. Zhang, Z. Zhu, S. Smith, M. Jaroniec, G. Q. M. Lu, S. Z. Qiao, *J. Am. Chem. Soc.* **2011**, *133*, 20116.
[16] S. M. Lyth, Y. Nabae, S. Moriya, S. Kuroki, M.-a. Kakimoto, J.-i. Ozaki, S. Miyata, *J. Phys. Chem. C* **2009**, *113*, 20148.
[17] S. M. Lyth, Y. Nabae, N. M. Islam, S. Kuroki, M. Kakimoto, S. Miyata, *J. Electroanal. Chem.* **2011**, *158*, B194.
[18] Y. Sun, C. Li, Y. Xu, H. Bai, Z. Yao, G. Shi, *Chem. Commun.* **2010**, *46*, 4740.
[19] E. Antolini, *Appl. Catal. B* **2009**, *88*, 1.
[20] H. Chang, S. H. Joo, C. Pak, *J. Mater. Chem.* **2007**, *17*, 3078.
[21] S. H. Joo, S. J. Choi, I. Oh, J. Kwak, Z. Liu, O. Terasaki, R. Ryoo, *Nature* **2001**, *412*, 169.
[22] A. Lu, A. Kiefer, W. Schmidt, F. Schuth, *Chem. Mater.* **2004**, *16*, 100.
[23] J. Fan, C. Yu, L. Wang, B. Tu, D. Zhao, Y. Sakamoto, O. Terasaki, *J. Am. Chem. Soc.* **2001**, *123*, 12113.
[24] H. I. Lee, G. D. Stucky, J. H. Kim, C. Pak, H. Chang, J. M. Kim, *Adv. Mater.* **2011**, *23*, 2357.
[25] Y. Meng, D. Gu, F. Zhang, Y. Shi, H. Yang, Z. Li, C. Yu, B. Tu, D. Zhao, *Angew. Chem.* **2005**, *117*, 7215; *Angew. Chem. Int. Ed.* **2005**, *44*, 7053.
[26] Y. Deng, T. Yu, Y. Wan, Y. Shi, Y. Meng, D. Gu, L. Zhang, Y. Huang, C. Liu, X. Wu, D. Zhao, *J. Am. Chem. Soc.* **2007**, *129*, 1690.
[27] C. Liang, S. Dai, *J. Am. Chem. Soc.* **2006**, *128*, 5316.
[28] W. Stober, A. Fink, E. Bohn, *J. Colloid Interface Sci.* **1968**, *26*, 62.
[29] H. Darmstadt, C. Roy, S. Kaliaguine, S. J. Choi, R. Ryoo, *Carbon* **2002**, *40*, 2673.
[30] S. H. Liu, J. R. Wu, *Int. J. Hydrogen Energy* **2011**, *36*, 87.
[31] L. Qu, Y. Liu, J. B. Baek, L. Dai, *ACS Nano* **2010**, *4*, 1321.
[32] H. S. Wroblowa, P. Yen Chi, G. Razumney, *J. Electroanal. Chem. Interfacial Electrochem.* **1976**, *69*, 195.
[33] M. T. de Groot, M. Merkx, A. H. Wonders, M. T. M. Koper, *J. Am. Chem. Soc.* **2005**, *127*, 7579.

